Quantification of Mechanical Deformations Induced by an Electric Field in a Semicrystalline Organic Insulator

P. R. Mamy,[1] J. Martinez-Vega,[1] J. C. Dupre,[2] N. Bretagne[2]

[1]*Laboratoire de Génie Electrique de Toulouse (UMR-CNRS 5003), Université Paul Sabatier, 118 Route de Narbonne, 31062 Toulouse Cedex, France*
[2]*Laboratoire de Mécanique des Solides (UMR-CNRS 6610), Bd Marie et Pierre Curie, Teleport 2, 86962 Futuroscope Chasseneuil Cedex, France*

Received 9 October 2003; accepted 18 March 2004
DOI 10.1002/app.20709
Published online in Wiley InterScience (www.interscience.wiley.com).

ABSTRACT: We studied mechanical deformations induced when an insulating material was subjected to a gradual increase in a direct-current electric field. Poly(ethylene terephthalate) film was studied with an optical technique, which was nondestructive and involved no physical contact. The experimental results indicated that the level of the induced mechanical deformation depended on the strength of the applied electric stress, the linear dimensions of the area under study, and the thickness of the film. When the studied area was relatively small, the level of the mechanical deformation seemed to be more important. The relationship between the induced mechanical deformation and the electric conduction phenomenon was also examined. © 2004 Wiley Periodicals, Inc. J Appl Polym Sci 93: 2313–2321, 2004

Key words: aging; dielectric properties; films; mechanical properties; thermoplastics

INTRODUCTION

This work falls within the framework of the study of the behavior of solid, organic insulating materials under an electric field when they are subjected to service conditions. We try to translate this behavior with a mechanical response when a solid insulating material is subjected to an electric field. Indeed, experimental studies carried out within the framework of the dielectric breakdown in organic insulating materials, as well as studies of the mechanical influence of electric stresses on solid insulating materials,[1–4] have highlighted the importance of the roles played by induced stresses in insulating material aging. They have established experimentally that these induced mechanical stresses are responsible for highly localized mechanical deformation in some polymer films.

For this reason, we decided to study, through experimentation, the mechanical response when a solid organic insulator was subjected to an electric field. The measurements were carried out at the ambient temperature (ca. 20°C) and for very short periods of time; this made it possible to minimize the environmental conditions. This study could also constitute a basis for the study of solid organic insulators under electric stress in normal use, when they are often associated with other stresses (thermal, mechanical, environmental, etc.). The mechanical response of the material is described in terms of induced mechanical deformations, which depend on the duration of the field application.

To carry out this work, we developed a device, and an experimental technique made it possible to follow in real time the mechanical behavior of a sample during the application of an electric field. Measurements were taken during the optical observation of a sample surface, and they provide information concerning the mechanical behavior during various stages of induced mechanical deformation. To compare the state of the electric-field-stressed material with its initial state (unstressed), we carried out the measurements in three stages: before, during, and after the setting under electric stresses. We also examined the effects of electric stresses, considering a relatively small measurement domain. This enabled us to introduce the concept of local fields while speaking about the part played by the relatively small regions in the behavior.

EXPERIMENTAL

Material and its morphological characterization

Poly(ethylene terephthalate) (PET) films provided by Dupont de Nemours Co. (Luxembourg) were studied. PET is a polymeric material in the family of thermoplastics, and it possesses a combination of physicochemical characteristics ideally suited to the manufacturing of the complex systems required in the electric and microelectronic industries. It is obtained from two basic products:

Correspondence to: J. Martinez-Vega (juan.martinez@lget.ups_tlse.fr).

Contract grant sponsor: Cooperation and Cultural Action Service of the France Embassy in Guinea (Conakry).
Contract grant sponsor: GdR ME²MS (through Opération Synergie des Contraintes et Durabilité des Isolants Organiques; CNRS-France).

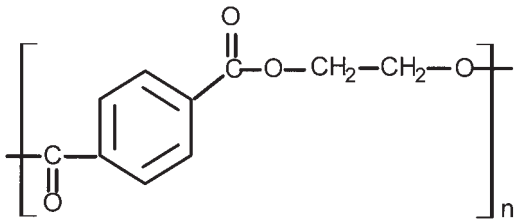

Figure 1 Chemical formula of PET.

ethylene glycol and terephthalic acid. The structure of PET can be amorphous or partially crystalline (up to 50%). The semicrystalline form is used a great deal (e.g., dielectrics in the manufacturing of capacitors). The chemical formula of PET is shown in Figure 1.

The rather low vitreous transition temperature (≈ 85°C) of PET is a handicap for its use in an amorphous state. At the passage of this temperature, the physical properties of PET vary strongly. This disadvantage is partially eliminated in a crystalline state, but thermal crystallization (in the vicinity of 150°C) is slow, and this increases the realization time. In the proximity of 250°C, the crystallites are destroyed by the thermal contribution of energy, and it corresponds to the melting temperature of PET.

We studied 25-, 36-, and 100-μm-thick PET semicrystalline films. To prepare a sample to be tested, we deposited a gold layer *in vacuo* with an S150B sputter coater. Two electrodes, 20 mm in diameter and 30 nm thick, were thus obtained on the two faces of a film; this made it possible to guarantee better electrode/polymer contact and to obtain a reflective surface. To eliminate the initial charges existing on the faces, we short-circuited each test sample for a few hours before the testing.

The mechanical properties of insulating materials depend on their morphology after implementation. To determine the morphology of the samples under study and the impact of gold metallization on the initial PET morphology, we analyzed two 25-μm-thick samples with differential scanning calorimetry (DSC): one was as-received (for the morphological study), and the other was gold-metalized (for the study of the effect of the metallization on the thermal properties of the material). The analyses were carried out under liquid nitrogen with specimens of about 13 mg; each sample was subjected to a rise in temperature from 30 to 290°C at 10°C/min.

The physical phenomena associated with the various phase transitions during the endothermic or exothermic processes were thus detected and quantified. This technique allowed us to determine the glass-transition temperature and melting temperature of each sample. The knowledge of the crystallization and melting enthalpies of the sample[5,6] allowed us to calculate directly the rate of crystallinity (χ_c). Figure 2 shows the DSC thermograms of the studied 25-μm-thick PET samples between 30 and 290°C, with the temperature increasing at rate of 10°C/min.

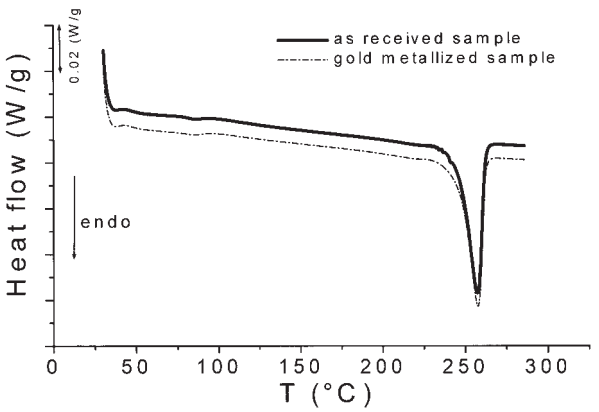

Figure 2 DSC thermograms of two PET samples (as-received and gold-metalized).

The thermograms in Figure 2 show practically no difference between the as-received and metalized samples. Moreover, the values given in Table I show very little difference, indicating in this case no appreciable effect of gold metallization on the morphological properties of the PET films.

Experimental device

As we mentioned previously, an optical technique was used. The induced mechanical deformations were quantified when a sample was subjected to electric stresses. For this study, we set up an experimental device; a functional diagram is shown in Figure 3. It included three essential parts: a sample-holder cell, which contained the sample to be tested, and two brass electrodes. The higher electrode of the cell was pierced with a 12-mm-diameter hole, which allowed the observation of the surface, whereas the lower electrode was used for the voltage application to the electric measurement circuit. The entire system was fed by a direct-current high-voltage source (HCN 35-20000) that delivered a maximum voltage of 20 kV and a current limited to 1.5 mA. An optical system, which included an optical microscope connected to a charge-coupled device (CCD) camera (resolution = 768 pixels × 576 pixels with 256 gray levels), permitted the observation of the sample surface in reflected light. A data-processing part gave control over the experiment.

TABLE I
Glass-Transition Temperature (T_g), Melting Temperatures (T_m) and Morphological Parameters of PET

Sample	T_g (°C)	T_m (°C)	ΔH_m (J/g)	χ_c (%)
As-received	82.6	257.4	42.85	35.8
Gold-metalized	82.5	257.6	42.7	35.7

ΔH_m = melting enthalpy.

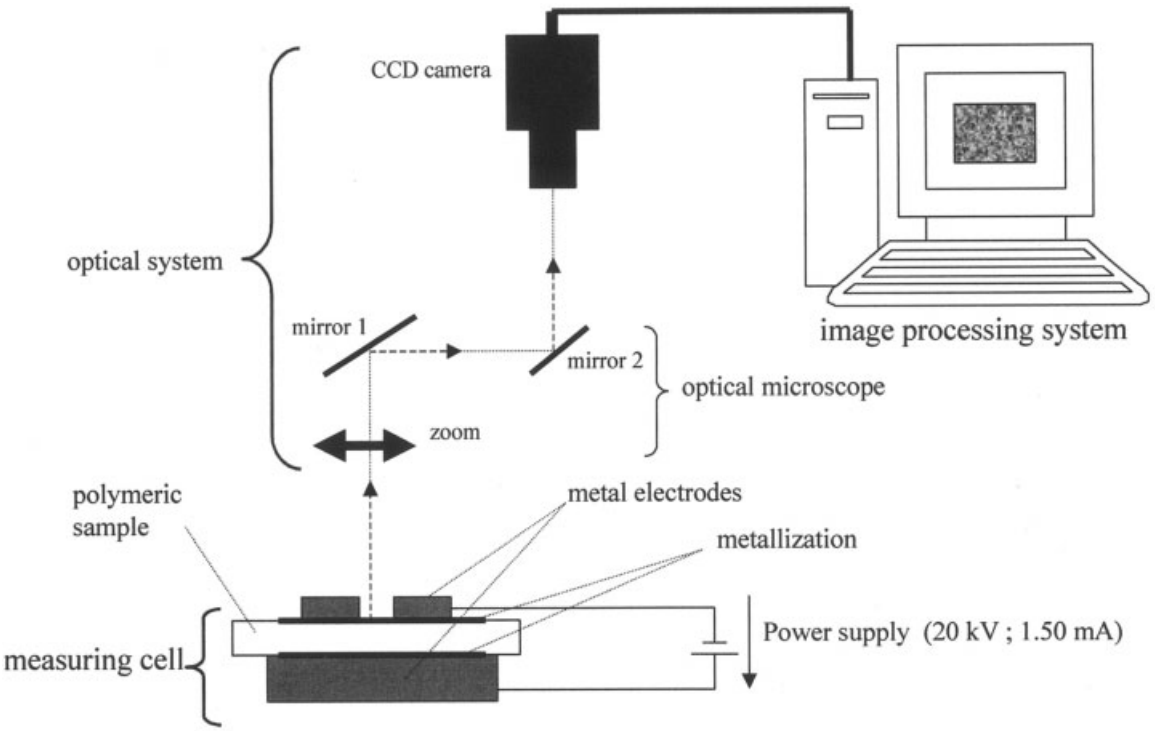

Figure 3 Functional diagram of the experimental device.

Using this device, we obtained an image of the gold-metalized surface of a sample (Fig. 4). The image reveals small, contrasting spots, which represent the microscopic light contrast of traditional metallization. To manipulate the test sample as little as possible, we identified four of these spots with computerized marking. The four markers thus obtained allowed us to quantify the mechanical deformation induced in real time by the applied electric field.

Principle of strain measurement

The principle of strain measurement[7–9] consists of four markers (Fig. 5), forming a cross, positioned on the sides of a parallelogram.

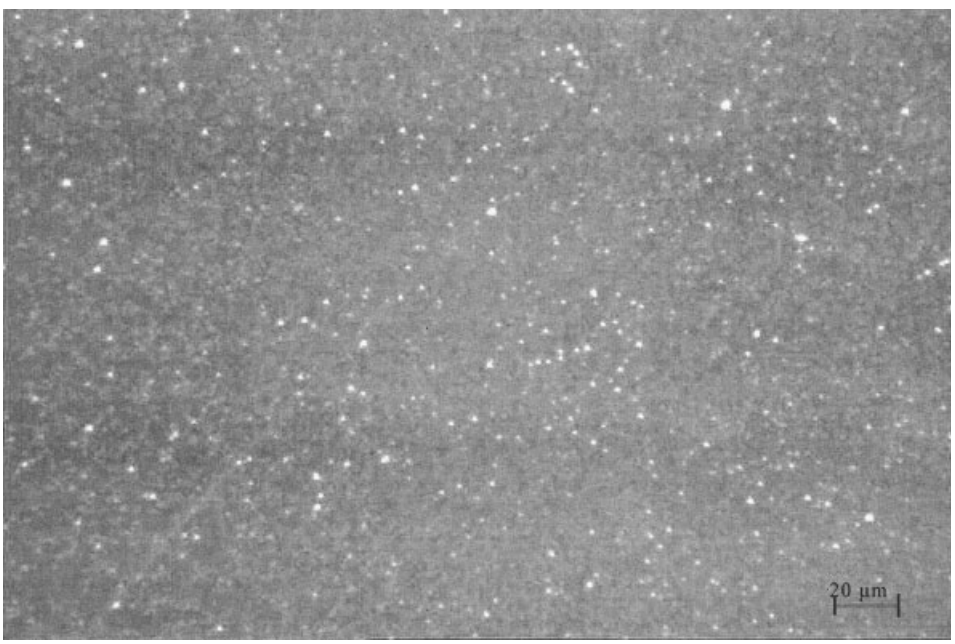

Figure 4 Image of a gold-metalized PET surface.

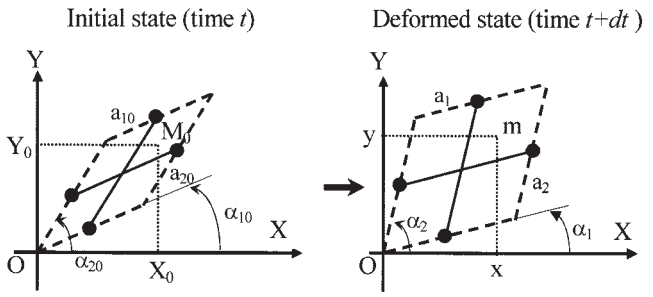

Figure 5 Schematic diagram of the follow-up of four markers.

Knowing the coordinates of these spots, at each state of loading, we can use the calculation of the lengths (a_1 and a_2) and orientations (α_1 and α_2) to determine, into a large deformation formulation, the Green–Lagrange strain tensor ($\bar{\bar{E}}$):[10]

$$\bar{\bar{E}} = \frac{1}{2}\left(\overline{\overline{F^M}}\ \overline{\overline{F^M}} - \bar{\bar{1}}\right) \tag{1}$$

where $\overline{\overline{F^M}}$ is the gradient tensor function of the following components:

$$\overline{\overline{F^M}} = \begin{bmatrix} \left(\dfrac{a_1 \cos\alpha_1 \sin\alpha_{20}}{a_{10}\sin(\alpha_{20}-\alpha_{10})} + \dfrac{a_2 \cos\alpha_2 \sin\alpha_{10}}{a_{20}\sin(\alpha_{10}-\alpha_{20})}\right) - \left(\dfrac{a_2 \cos\alpha_2 \cos\alpha_{10}}{a_{20}\sin(\alpha_{10}-\alpha_{20})} + \dfrac{a_1 \cos\alpha_1 \cos\alpha_{20}}{a_{10}\sin(\alpha_{20}-\alpha_{10})}\right) \\ \left(\dfrac{a_1 \sin\alpha_1 \sin\alpha_{20}}{a_{10}\sin(\alpha_{20}-\alpha_{10})} + \dfrac{a_2 \sin\alpha_2 \sin\alpha_{10}}{a_{20}\sin(\alpha_{10}-\alpha_{20})}\right) - \left(\dfrac{a_2 \sin\alpha_2 \cos\alpha_{10}}{a_{20}\sin(\alpha_{10}-\alpha_{20})} + \dfrac{a_1 \sin\alpha_1 \cos\alpha_{20}}{a_{10}\sin(\alpha_{20}-\alpha_{10})}\right) \end{bmatrix} \tag{2}$$

The experimental technique makes it possible to measure five induced mechanical deformation components associated with the plane surface of a film. We label these components ϵ_x, ϵ_y, and γ_{xy}, which are associated with the directions parallel to the *x*-, *y*-, and *xy*-shearing axes, respectively. The ϵ_1 and ϵ_2 components are associated with the principal directions at which γ_{xy} is null. We have assumed the homogeneity of the deformation on the measurement base, and as a result, the reported values are averages.

The principle of mark tracking is to calculate the geometric center of the spot from a rectangular zone (the research zone), defined at the beginning of the computation, around each spot by its upper left coordinates (x_z, y_z) and size (N_x, N_y). For large deformations and movements, this research zone is automatically moved at each step of time, with consideration given to the measured displacement, to keep the spot inside.

Then, the coordinates (x_g and y_g) of each marker are derived with the following equations:

$$\begin{cases} x_g = \dfrac{\sum_{x=0}^{N_x}\sum_{y=0}^{N_y} x[I(x,y) - I_s]}{\sum_{x=0}^{N_x}\sum_{y=0}^{N_y}[I(x,y) - I_s]} + x_z \\ y_g = \dfrac{\sum_{x=0}^{N_x}\sum_{y=0}^{N_y} y[I(x,y) - I_s]}{\sum_{x=0}^{N_x}\sum_{y=0}^{N_y}[I(x,y) - I_s]} + y_z \end{cases} \tag{3}$$

where I_s is the lower limit of the light intensity (beyond this limit, the pixel is not discriminated) and $I(x,y)$ is the light intensity of the pixel with coordinates x and y.

Protocol

We applied a gradual direct-current voltage increase from 0 to 8 kV (Fig. 6), with steps of 1 kV (without depolarization), to quantify the mechanical deformations induced during a gradual increase of the electric field. The application time of a voltage step was fixed at 200 s. After the test, we removed the electric stress to study the return of the material to its original state. To obtain measurement reproducibility, we carried out measurements of the noise levels before the application of the electric field for a certain period.

RESULTS

Noise level measurements

Performance of the strain measurement

The accuracy of the strain measurement is a function of the marker position and the distance between the

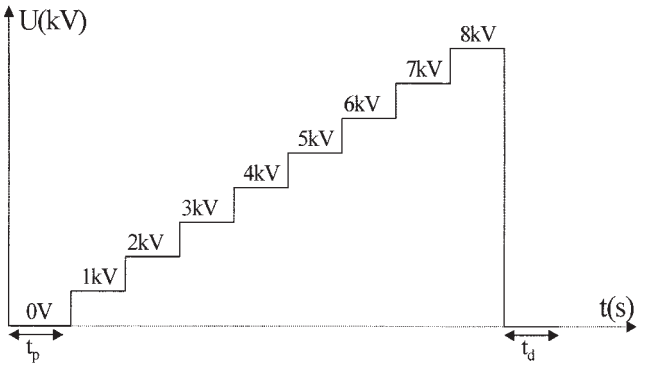

Figure 6 Schematic diagram of the experimental protocol. t_p is the time for the step voltage application, and t_d is the removal voltage time ($t_p = t_d = 200$ s).

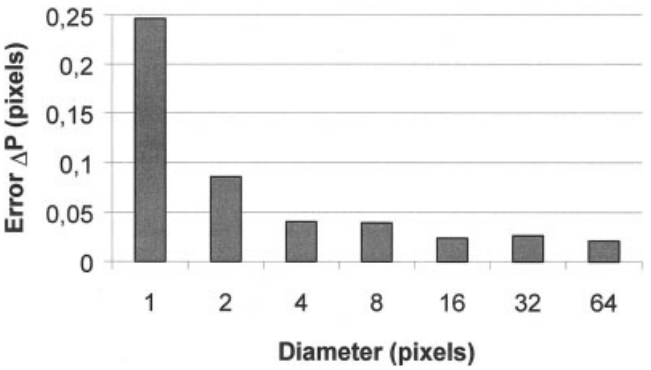

Figure 7 Error on the marker position function with respect to its size.

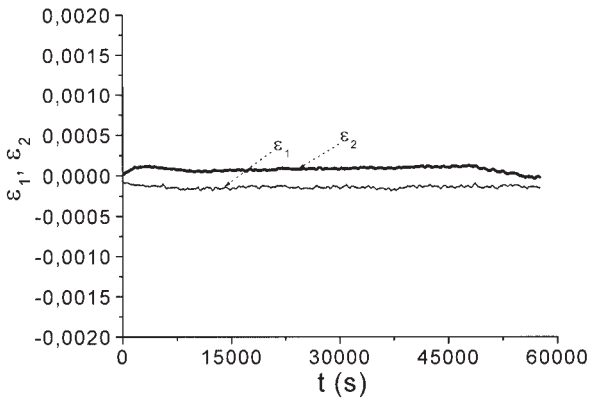

Figure 9 ϵ_1 and ϵ_2 components of the noise levels corresponding to the distant markers (electric field = 0);

spots. Experimental tests were performed to determine the performances of the marker tracking technique.

We used circular markers. The experimental procedure consisted of applying an in-plane displacement to a specimen (with several markers) with a micrometric translation stage (1 step = 0.02 pixels). In Figure 7, we show the results of our technique. The error (ΔP) decreases with the diameter (d) of the markers: $\Delta P = 0.1$ pixels for $d = 2$ pixels and $\Delta P < 0.05$ for $d > 4$ pixels.

To study the accuracy of the deformations, we can determine the strain in one direction, with the first approach (small perturbation hypothesis), from the distance (l) between two markers and the distance in the initial state (l_0):

$$\varepsilon = \frac{l - l_0}{l_0} \tag{4}$$

Under a small strain, we assume $l_0 \approx l \gg l - l_0$. Therefore, we obtain

$$\frac{\Delta\varepsilon}{\varepsilon} = \frac{\Delta l + \Delta l_0}{l - l_0} \Rightarrow \Delta\varepsilon = \frac{\Delta l}{l_0} + \frac{\Delta l_0}{l_0} = \frac{2\Delta l}{l_0} = \frac{4\Delta p}{l_0} \tag{5}$$

For $l_0 = 500$ pixels, we obtain $\pm 4 \times 0.05/500 = \pm 4 \times 10^{-4}$ for small spots ($d = 4$ pixels) and $\pm 2 \times 10^{-4}$ for large spots (ca. 16 pixels). The precision decreases to $\pm 4 \times 0.05/50 = \pm 4 \times 10^{-3}$ if the distance between the two marks becomes 50 pixels.

Noise level measurement for this application

The aforementioned accuracy was obtained for spots made with a fine pen, and an experimental test was carried out to see if for this new application the accuracy was similar. The measurements of the noise level were carried out for an as-received PET sample 25 μm thick on a mechanical deformation scale for 16 h without an electric field.

Figures 8–11 show the measured components of the noise levels corresponding to the distant markers (average distance $d_1 \approx 213$ μm between 200 and 227 μm, ca. 500 pixels; Fig. 12) and to the close-in markers

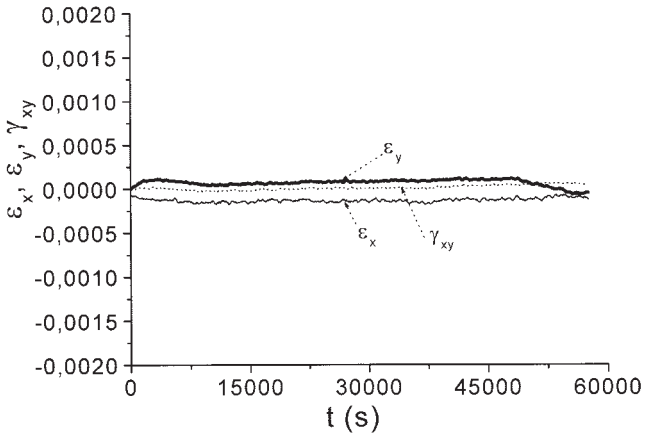

Figure 8 ϵ_x, γ_{xy}, and ϵ_y components of the noise levels corresponding to the distant markers (electric field = 0);

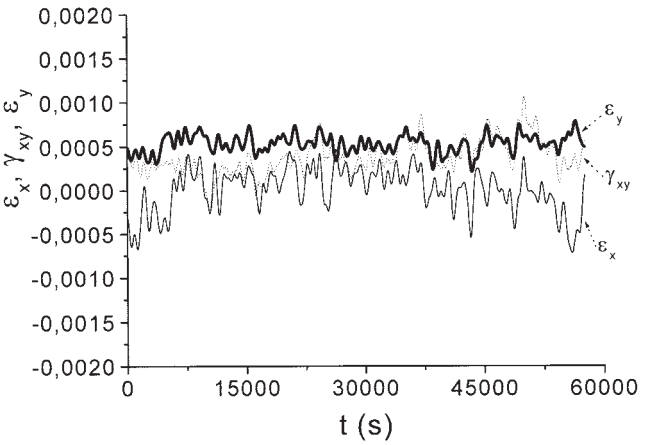

Figure 10 ϵ_x, γ_{xy}, and ϵ_y components of the noise levels corresponding to the close-in markers (electric field = 0).

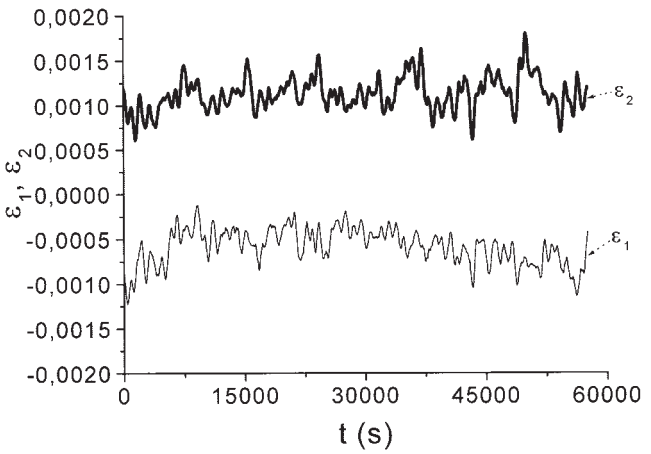

Figure 11 ϵ_1 and ϵ_2 components of the noise levels corresponding to the close-in markers (electric field = 0).

(average distance $d_2 \approx 28$ μm between 20 and 37 μm, ca. 50 pixels; Fig. 13).

These figures show that in both cases the noise levels were very small and corresponded to the predicted error (ca. 2×10^{-4} for large distances and 10^{-3} for small distances). Moreover, for the higher electrode used in these measurements, which was pierced with a hole 12 mm in diameter and had an external diameter of 18 mm; its mass m was estimated to be approximately 10 g. The mechanical stress that this electrode could induce in a PET film 25 μm thick was about 707 Pa. The preceding calculations showed clearly that we could neglect the effect of the weight of the higher electrode. The measured mechanical deformations in our work thus corresponded only to the mechanical strain induced by the electric field application.

Quantification of the induced mechanical deformations under electric field applications

Case of a distant marker configuration

We initially considered the distant marker configuration previously mentioned. This configuration corresponded to a large observation area of the surface visualized by the optical observation system of our experimental device. Figures 14 and 15 show the evolution of the two component spectra of the mechanical response of a test PET sample during the experimental phase.

Figure 14 shows a gradual increase in the mechanical deformations ϵ_x and γ_{xy} and a lower evolution of ϵ_y with the applied electric field. These components are related to the image plane of the CCD camera. Components ϵ_2 and ϵ_1 evolved similarly to components ϵ_x and ϵ_y. We had to use a diagonal form of the strain tensor for our study of the mechanical response of the sample (see Fig. 15).

We studied the contributions of ϵ_1 and ϵ_2 to the total mechanical deformation of a PET sample. Indeed, ϵ_1 and ϵ_2 were measured along two directions associated with the analyzed local surface. We considered them the components of the vector of deformation, the modulus (ϵ') of which was obtained as follows:

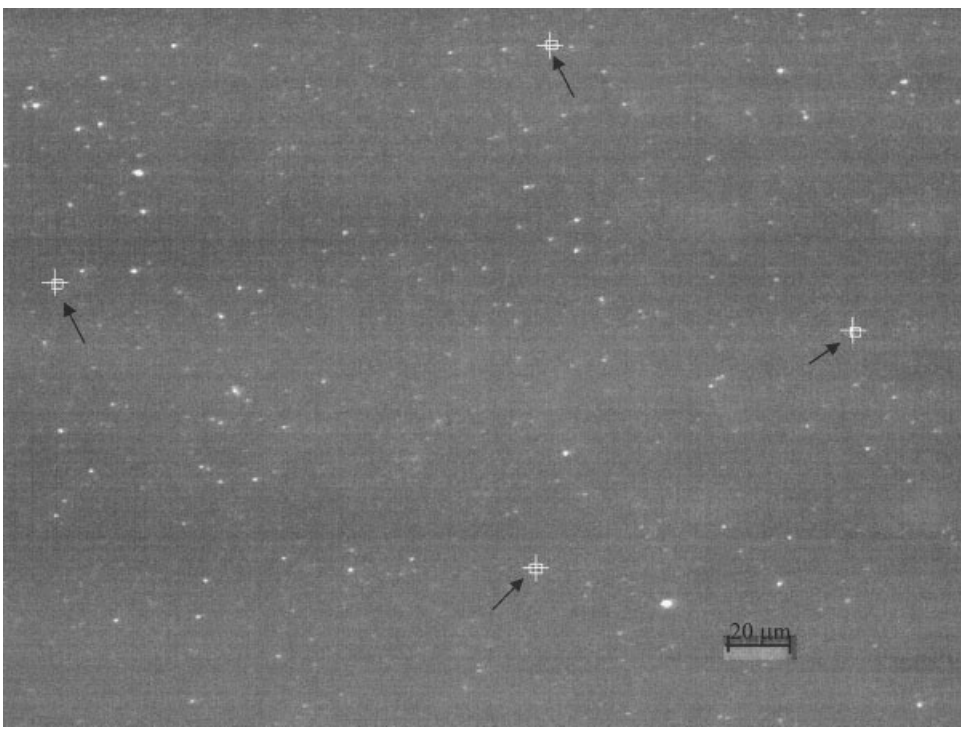

Figure 12 Configuration of the distant markers (average distance of 213 μm between 200 and 227 μm).

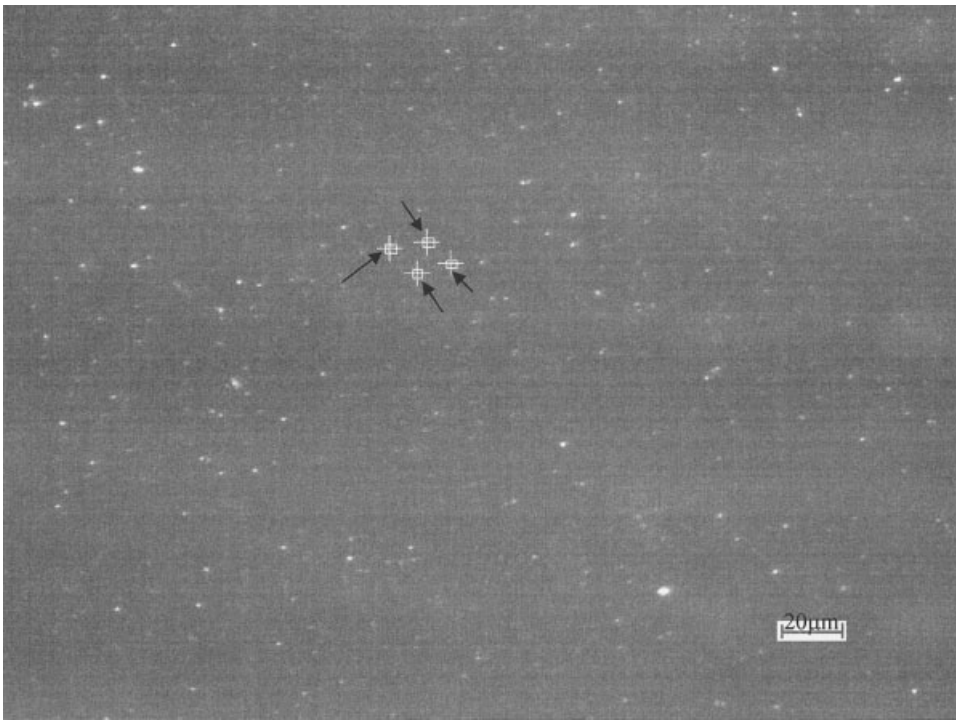

Figure 13 Configuration of the close-in markers (average distance of 28 μm between 20 and 37 μm).

$$\varepsilon' = (\varepsilon_1^2 + \varepsilon_2^2)^{\frac{1}{2}} \quad (6)$$

A representation of ϵ' versus an electric field is shown in Figure 16. The total mechanical deformations (i.e., ϵ') were relatively small for fields of 0–120 V/μm ($<10^{-3}$). Moreover, we observed that above 160 V/μm, the mechanical deformations increased more quickly as the electric field increased. The slopes of the curve corresponding to both areas, zones I and II, intersected at a point of the abscissa around an electric field of 160 V/μm, and it should define a kind of threshold field, that is, the electric field from which the deformation increased quickly.

To accurately determinate the value of the field threshold and the characteristic properties of ϵ', we carried out in an analogous fashion the conduction current measurements.

The result diagram (Fig. 17) shows the existence of two domains of the electric field, which could correspond to two zones of mechanical deformation. The first one, so-called zone I, corresponded to the linear (ohmic) zone, in which the conductivity of the sample

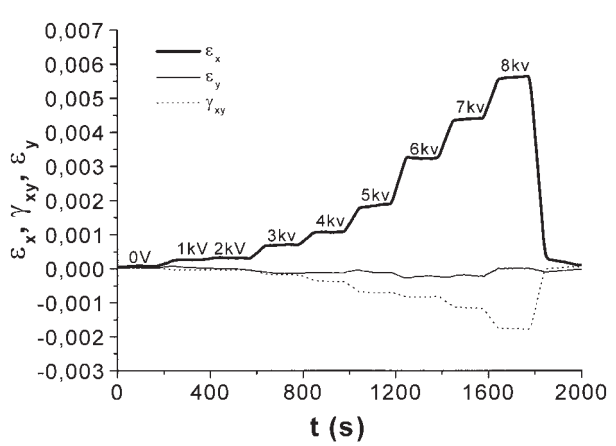

Figure 14 ϵ_x, γ_{xy}, and ϵ_y components of the temporal mechanical response of a 25-μm-thick PET sample corresponding to the distant marker configuration (average distance between 200 and 227 μm).

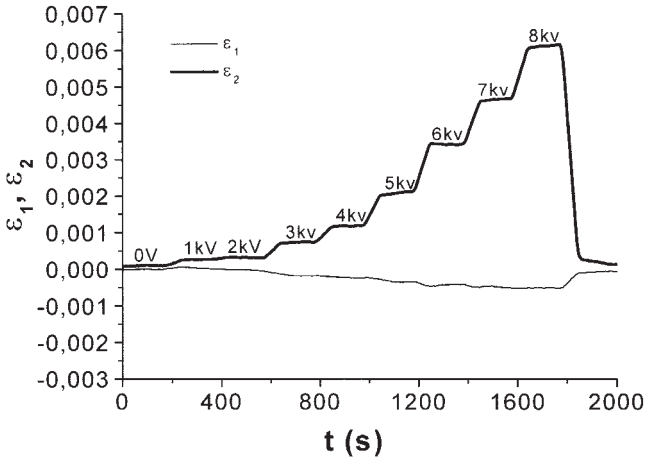

Figure 15 ϵ_1 and ϵ_2 components of the temporal mechanical response of a 25-μm-thick PET sample corresponding to the distant marker configuration (average distance between 200 and 227 μm).

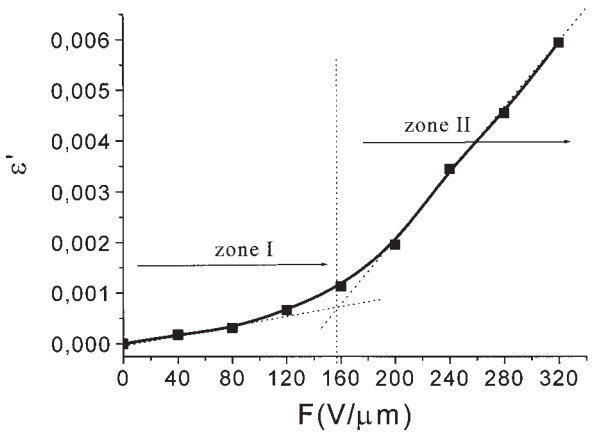

Figure 16 Electric field (F) dependence of ϵ' for a sample 25 μm thick.

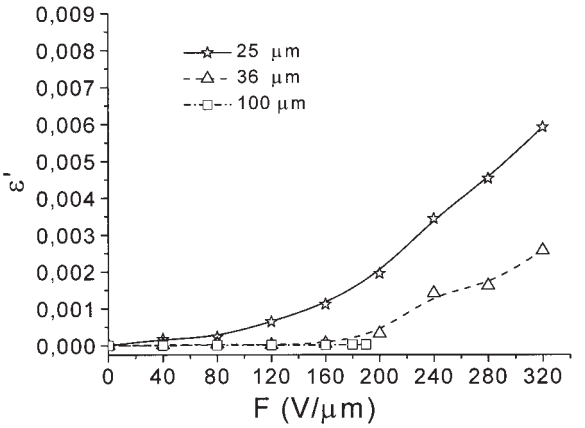

Figure 18 Electric field (F) dependence of ϵ' for three PET samples 25, 36, and 100 μm thick.

had a linear response with respect to the electric field; the second one was associated with relatively higher fields, in which the current increased in a nonlinear way with the electric field. This second zone could correspond to a deformation level higher than 10^{-3}. The threshold of the two zones in the mechanical deformation case was about 160 V/μm. This shows that the physical mechanisms were related in both mechanical and dielectric cases.

Moreover, during the mechanical deformation measurements under an applied electric field, in the second zone, a cracking noise was often heard during passage through 4.50 kV (corresponding to an electric field of 180 V/μm), and it corresponded in several cases to a beginning of demetalization in a 25-μm-thick PET film. This means that this magnitude of voltage was critical for this thickness because it could cause damage if the sample was exposed a long time to the applied stress.

A study of the electric dependence of the mechanical deformation for three PET films 25, 36, and 100 μm thick (Fig. 18) indicated a strong dependence of the induced mechanical deformation on the thickness of the PET films.

Figure 15 shows that the sample 25 μm thick deformed more rapidly under small fields than 36- and 100-μm-thick films. For the sample 36 μm thick, the mechanical deformation began to increase around 160 V/μm and corresponded to a deformation level of about 1.08×10^{-4}; this field could also correspond to the threshold of the sample 25 μm thick. On other hand, for the 100-μm-thick film, these parameters were not specified in the considered electric field range. Figure 18 shows clearly that there was a thick-film effect. This effect was certainly related to the different morphologies associated with each thick film used.

Case of a close-in marker configuration

Several studies and models have highlighted the roles of microdomains in the aging mechanism and dielectric breakdown of insulating materials.[11,12] The dielectric breakdown of insulating materials can be well

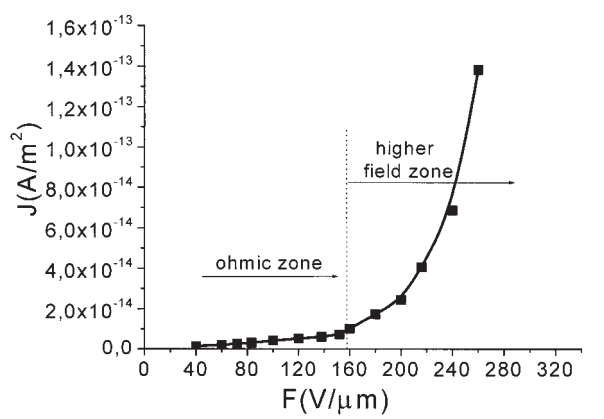

Figure 17 Electric field (F) dependence of the current conduction (J) in a PET sample 25 μm thick.

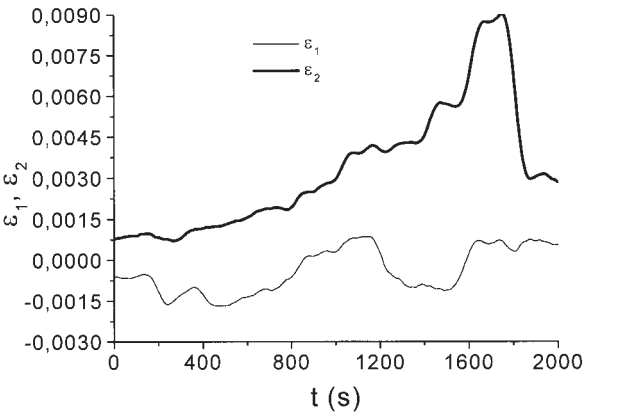

Figure 19 Temporal mechanical response of a 25-μm-thick PET sample corresponding to the close-in markers (average distance between 20 and 37 μm).

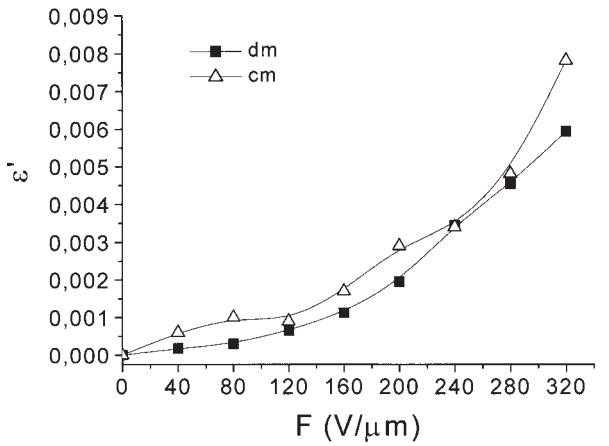

Figure 20 ϵ' versus the electric field (F) for both distant (dm) and close-in (cm) marker configurations.

explained by very reduced zones, which can be associated with the concept of local fields. In this way, we decided that it was useful to study the influence of a gradually increasing electric field on a reduced zone, defined in our case by the close-in marker configuration. Thus, on the basis of a previous image-acquisition program used for the distant marker configuration measurements (average distance ranging from 200 to 227 μm between distant markers) and with the same images, we chose another four markers corresponding to a close-in marker configuration. Therefore, we quantified the induced mechanical deformations in a reduced zone defined by the markers with an average distance between 20 and 37 μm. The components of the mechanical response obtained in this case are shown in Figure 19.

To analyze the effects induced by the electric field by taking account of the surfaces defined by these markers, we present in Figure 20 a diagram of the total deformations corresponding to both marker configurations, distant and closer-in.

Figure 20 indicates a difference between the total deformations corresponding to both cases, distant and closer-in. In the entire field range, from 40 to 320 V/μm, the total deformation for the closer-in markers tended to be higher than that corresponding to distant markers. This tendency could be explain by the possible existence of a local field. In this work, we can speak only of a tendency because even in our close-in marker configuration ($\approx$28 μm), the distance was too important, and we cannot speak about the local field. This track could be exploited and discussed in another article.

CONCLUSIONS

In this study, we highlighted the mechanical response of PET films under gradually increasing electric fields through the quantification of the induced mechanical deformations. This study was carried out with an optical technique that did not involve physical contact, and it was based on the follow-up of four markers on a sample surface. Two configuration marker types were studied: distant and close-in. The experimental results obtained for the distant markers showed good resolution and an increase in the induced mechanical deformation with a gradual increase in the applied electric field. Moreover, a study of the mechanical deformation for three PET films (25, 36, and 100 μm thick) indicated a strong thickness dependence (morphology effect) of the mechanical deformation and threshold field.

In the case of the close-in markers, a higher deformation level was obtained than that of the distant markers. This showed a certain tendency: the mechanical deformation was higher when the markers were closer. This tendency could be explained by the possible existence of a local field.

We studied the properties of the mechanical characteristic ϵ' by measuring the electric conduction current, and we obtained a good approximation for the field threshold, around 160 V/μm, from the results.

This study allowed us to examine the mechanical response of insulating materials under an electric field, and it constitutes a solid base for the study of the behavior of solid insulating materials used under electric fields or multistress operating conditions, in which several stresses are involved.

References

1. Blok, J.; LeGrand, D. G. J Appl Phys 1969, 40, 288.
2. Nishijima, S.; Hara, M. Cryogenics 1998, 38, 1105.
3. Liu, C.; Bar-Cohen, Y.; Leavy, S. ESSP Proceedings of SPIE's 6th Annual International Symposium on Smart Structures and Materials, Newport Beach, CA, March 1999; Paper 3669-41, p 1.
4. Perline, R.; Kornbluch, R.; Joseph, J.; Heydt, R.; Pei, Q.; Chiba, S. Mater Sci Eng C 2000, 11, 89.
5. Kitano, Y.; Kinoshita, Y.; Ashida, T. Polymer 1995, 36, 1947.
6. Evstatiev, M.; Fakirov, S.; Apostolov, A. Polym Eng Sci 1992, 32, 964.
7. Brémand, F.; Dupré, J. C.; Lagarde, L. Photomécanique 1995, 95, 171.
8. Rotinat, R.; Tiébi, R.; Valle, V.; Dupré, J. C. Strain 2001, 37, 89.
9. Bretagne, N.; Dupré, J. C. Presented at the 15th French Congress of Mechanics, Nancy, France, Sept 2001.
10. Naday, A. Theory of Flow and Fracture of Solids; McGraw-Hill: New York, 1950.
11. Lewis, T. J. IEEE Electr Insul Mag 2001, 17, 6.
12. Zurkov, S. N.; Kursokov, A. F. J Polym Sci Polym Phys Ed 1974, 12, 385.